

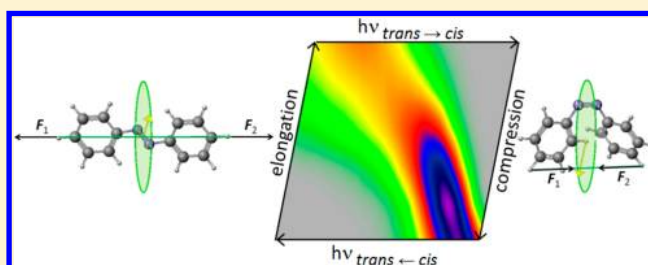
Toward an Optomechanical Control of Photoswitches by Tuning Their Spectroscopical Properties: Structural and Dynamical Insights into Azobenzene

Felipe Zapata, Miguel Ángel Fernández-González, Daniel Rivero, Ángel Álvarez, Marco Marazzi,^{*,†} and Luis Manuel Frutos^{*}

Departamento de Química Analítica, Química Física e Ingeniería Química, Universidad de Alcalá, E-28871 Alcalá de Henares, Madrid, Spain

S Supporting Information

ABSTRACT: A new methodology to calculate efficiently the absorption spectrum of a single molecule when subjected to mechanical stress is presented. As example, the developed methodology was applied to *cis*- and *trans*-azobenzene, commonly used as photoswitch in a wide variety of applications. The results show that both $^1(n,\pi^*)$ and $^1(\pi,\pi^*)$ optical transitions can be efficiently modulated by applying an external force. A structural analysis was performed to evaluate the role of each internal coordinate in the excitation process, taking into account the application of external forces at different positions of azobenzene. Moreover, stress–strain curves were calculated in order to determine the maximum applicable forces within the elastic region, highlighting notable differences between the mechanical properties of *cis*- and *trans*-azobenzene conformers. The optomechanical work obtained by elongation and compression steps is calculated for a single azobenzene molecule and compared to available experimental data. Finally, the implications derived from the application of azobenzene as main chain component of a linear polymer acting as a photoinduced motor are discussed.



INTRODUCTION

Optomechanics is a modern multidisciplinary field of science in which fundamental aspects have been discovered in the past decade, outlying important challenges and perspectives for the future. Optomechanical materials are based on direct conversion of light (applied as input) into macroscopic motion. This behavior, in turn, depends on the molecular structure of the material itself. Especially, soft organic materials were successfully designed as optomechanical responsive systems (e.g., oligomers and polymers) where the presence of one or more chromophore units is essential to ensure light absorption, which constitutes the first necessary event to promote the subsequent conformational and/or chemical modification underlying mechanical motion.^{1,2}

Photoswitches are bistable (state A and B) chromophores of special interest in the design and fabrication of optomechanical devices, since the absorption of light at a certain wavelength by state A is usually followed by a large structural change, which makes it possible to reach state B. Then a second pulse of light (or thermal relaxation step), commonly at a different wavelength, reverses the process defining a pathway from state B back to state A.^{3,4} Specifically, switches based on photoisomerization are commonly applied to solve a variety of scientific and engineering problems, ranging from protein conformation control to photocatalysis, from molecular data storage to foldamers. In all these cases, photoisomerization

provides an efficient (i.e., ultrafast time scale) way to switch a process ON and OFF.⁵

Moreover, we can take advantage of the photoswitching property of a chromophore by generating optomechanical work in a single molecule device, operating switching cycles in a periodic mode, and therefore leading to the eventual design and fabrication of optomechanical motors.^{6–10}

Here, we focus on the photophysical step of the cycle (i.e., absorption of light) aiming to control spectroscopical properties once the switch is subject to external forces in an applied environment (e.g., covalently bound to a protein or peptide,^{11,12} or introduced in the main chain of liquid crystal polymer systems^{13,14}). More generally, in this study, we present a new and efficient method to simulate single molecule force spectroscopy of whatever chromophore. We show its application to (*cis* and *trans*) azobenzene, being one of the most studied and applied photoisomerizable switch.^{15–20}

The paper is organized as follows: first, the proposed theoretical methods are presented, especially the ground state molecular optimization and dynamics schemes, necessary for the simulation of the absorption spectra, the structural analysis required to determine which internal coordinates are more involved in the modulation of the excitation energy (including

Received: August 29, 2013

Published: December 19, 2013

the application of different sets of external forces), the simulation of single molecule stress–strain curves and the calculation of optomechanical work and power. This is followed by a description of the results obtained when applying the proposed methods to azobenzene. Therefore, azobenzene ground state topology is studied first, followed by an evaluation of its mechanical properties. This allows us to estimate the maximum applicable force to both *cis* and *trans* conformers, within the elastic region. The spectra recorded when applying a different set of forces are shown, indicating a relevant force induced modulation of spectroscopical properties (shift of the maximum absorption wavelength, broadening of the peak, change of absorption intensity), which can be useful in designing new optomechanical tools at a low computational cost. The main coordinates involved in the observed bathochromic and hypsochromic shifts are found, and the application of external forces at different positions of azobenzene is proposed. Finally, we discuss the possible implications derived from the introduction of azobenzene as main chain component of a linear polymer,^{21–24} especially focusing on maximizing the optomechanical work and power, which could be obtained by applying the highest possible deforming force compatible with the mechanical tests performed.

THEORETICAL METHODS

Force-Induced Ground State Molecular Optimization and Dynamics. Recently, a growing interest was shown by the theoretical chemistry and physics communities in order to describe adequately the behavior of molecules when an external force is applied to selected pairs of nuclei. Especially, we should mention the work of Martinez and co-workers, who explained relevant mechanochemical processes (e.g., force induced rupture of covalent bonds) through “on the fly” *ab initio* steered molecular dynamics (AI-SMD) simulations.^{25–27} Almost at the same time, Wolinski et al. proposed a method for geometry optimization in presence of external forces.^{28,29}

In this study, we propose an alternative approach by which extensive dynamics simulations can be performed, since energy and forces are not evaluated at each step of the simulation (as for the “on the fly” approach), being classical molecular dynamics performed on a previously constructed analytical potential energy surface (PES). Among the different possible approaches for building an analytical PES, we opted for a simple quadratic expansion centered on the minimum energy structure of *cis* (and *trans*) azobenzene (see for details the section Azobenzene Topology and Supporting Information), which can be calculated as follows:

$$E_{\text{GS}}(\mathbf{q}) = E_{\text{GS}}(\mathbf{q}^{\text{eq}}) + \frac{1}{2}(\mathbf{q} - \mathbf{q}^{\text{eq}})^{\text{T}} \mathbf{H}_{\text{GS}}(\mathbf{q} - \mathbf{q}^{\text{eq}}) \quad (1)$$

where E_{GS} is the energy in the ground state (GS) as a function of the molecular configuration in internal coordinates \mathbf{q} , being \mathbf{q}^{eq} the vector corresponding to the minimum energy (i.e., equilibrium) structure in the GS. Whatever displacement from \mathbf{q}^{eq} corresponds to energy increase, as indicated by the second term on the right-hand side of eq 1, being \mathbf{H}_{GS} the ground state Hessian matrix numerically calculated for the equilibrium geometry (the energy gradient is a null vector).

Classical molecular dynamics simulations were computed on the constructed ground state PES, applying the following methodology: a canonical ensemble was reproduced by expanding the current Hamiltonian through the Nosé–Hoover

method, which permits to include in the Hamiltonian the required degrees of freedom to simulate a thermostat.³⁰ This results in a canonical distribution of the molecular system. The Newtonian equations of motion were integrated by a time reversible integrator, applying the Liouville approach through the Trotter factorization.³¹ External forces are included by adding to the force vector determined from the analytical PES at each step of the dynamics, constant force vectors applied to selected pairs of nuclei. In our case, the pair of external force vectors was applied to the two hydrogen atoms of the benzene rings in *para* position with respect to the N=N moiety, in order to simulate the usual environment of azobenzene as a photoswitch in peptides and as main chain component of linear polymers. The direction of the external force is therefore the line connecting the two selected atoms, having both force vectors the same modulus. This leads to two possible mechanical stresses: elongation and compression. Both were considered as acting stresses over azobenzene (see Figure 5). In order to test the results obtained by the dynamical treatment, and as an additional method to estimate azobenzene structure under a static stress, force constrained optimizations were performed applying a quasi Newton–Raphson modified method, where at each step the external force is introduced by updating the calculated energy gradient (see Supporting Information for details).

Simulation of the Absorption Spectra. The same approach used to construct the ground state PES can be applied to build an electronic excited state PES:

$$E_{\text{ES}}(\mathbf{q}) = E_{\text{ES}}(\mathbf{q}^{\text{eq}}) + (\mathbf{q} - \mathbf{q}^{\text{eq}})^{\text{T}} \mathbf{g}_{\text{ES}} + \frac{1}{2}(\mathbf{q} - \mathbf{q}^{\text{eq}})^{\text{T}} \mathbf{H}_{\text{ES}}(\mathbf{q} - \mathbf{q}^{\text{eq}}) \quad (2)$$

where E_{ES} is the energy, \mathbf{g}_{ES} the energy gradient vector, and \mathbf{H}_{ES} the Hessian matrix, numerically calculated for the excited state (ES). The quadratic expansion in eq 2 is therefore centered on the same ground state equilibrium geometry (\mathbf{q}^{eq} , i.e. the Franck–Condon geometry) as in eq 1.

Following this approximation for the ES PES, the excitation energy can be determined at each step of a molecular dynamics simulation performed on the GS PES; that is, each step of the trajectory corresponds to a ground state and an excited state energy value, which difference is a vertical excitation energy: $E_{\text{ES}}(\mathbf{q}) - E_{\text{GS}}(\mathbf{q})$ (see Figure 1). Therefore, if the dynamics run

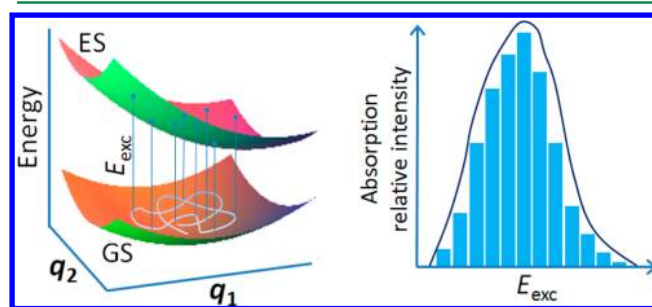


Figure 1. Left: schematic potential energy surfaces of the electronic ground state (GS) and excited state (ES) for a chromophore, as a function of two of its coordinate (q_1 , q_2); a ground state trajectory is depicted, with some of the corresponding vertical excitation energies (E_{exc}). Right: absorption spectrum, calculated as a histogram of relative intensity as a function of E_{exc} resulting from each geometry of the ground state trajectory.

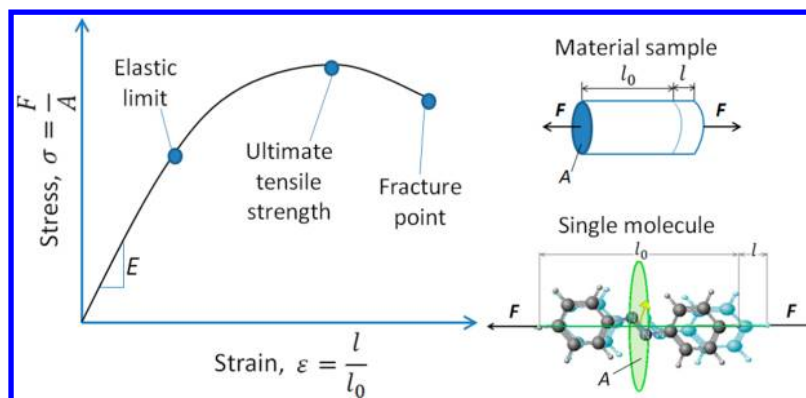


Figure 2. Example of a stress–strain curve, showing typical magnitudes of interest (left). A comparison between macroscopic and proposed microscopic samples is given (right).

is long enough to sample correctly the ground state PES at a given temperature, and if the quadratic approximation can be considered valid for both ground and excited states, the absorption spectrum corresponding to the GS \rightarrow ES electronic transition is simulated. More in detail, the following procedure was adopted for calculating the absorption spectrum: as first, the lowest and the highest vertical excitation energies recorded during the dynamics determine the width of the spectrum. Such width is then divided into equal intervals of energy, defining the sensitivity of the spectrum. Finally, each vertical excitation energy computed during the trajectory is assigned to the corresponding energy interval. Therefore, the absorption spectrum results in a histogram of relative intensity as a function of the excitation energy, where the relative absorption intensity of a given interval is proportional to the oscillator strength (i.e., to the transition dipole moment) and to the number of structures of the trajectory presenting an excitation energy falling in this interval (see Supporting Information for details).

The proposed methodology permits to perform dynamics simulations in the picosecond-time-scale in few hours of computation, correctly sampling the phase-space and providing a consistent prediction of the absorption spectrum at a determined constant temperature.

Structural Analysis. A rational modulation of the shift in absorption energy under external stress was considered, based on the development of an algorithm to minimize or maximize the energy gap between ground and selected excited states. Especially, the following question can be answered: provided only the magnitude of the applied external force, which is the specific force vector (i.e., the components for each nucleus) that causes the highest (bathochromic and hypsochromic) shift in the absorption energy? Alternatively, an equivalent question is the following: provided a given shift of the excitation energy, which is the external force vector with the lowest magnitude yielding such a shift? To answer this question, a restrained optimization has to be performed, where the Lagrangian function is defined as:

$$L = |\nabla E_{\text{GS}}|^2 + \lambda(\Delta E_{\text{exc}} - k) \quad (3)$$

where the function to be optimized is the squared energy gradient vector of the ground state PES subject to the condition that the excitation energy is equal to a given value: $\Delta E_{\text{exc}} = k$, and where λ is the corresponding Lagrange multiplier. The coordinates of the shifted structure can be found by optimizing the Lagrange function:

$$\nabla L = 2\mathbf{H}_{\text{GS}}^2 \mathbf{q}_{\text{opt}} + \lambda[\mathbf{g}_{\text{ES}} + (\mathbf{H}_{\text{ES}} - \mathbf{H}_{\text{GS}}) \mathbf{q}_{\text{opt}}] = 0 \quad (4)$$

which can be rearranged in the form:

$$\left(\frac{2}{\lambda} \mathbf{H}_{\text{GS}}^2 - \mathbf{H}_{\text{GS}} + \mathbf{H}_{\text{ES}} \right) \mathbf{q}_{\text{opt}} = -\mathbf{g}_{\text{ES}} \quad (5)$$

If $\mathbf{A} = 2/\lambda \mathbf{H}_{\text{GS}}^2 - \mathbf{H}_{\text{GS}} + \mathbf{H}_{\text{ES}}$ and $\mathbf{b} = -\mathbf{g}_{\text{ES}}$, it follows that $\mathbf{q}_{\text{opt}} = \mathbf{A}^{-1} \mathbf{b}$. The optimized structure \mathbf{q}_{opt} corresponds to the molecular configuration resulting from the application of a minimal external force giving rise to the desired excitation energy shift. Obviously, the optimal external force vector is known, since it equals the energy gradient of the ground state ∇E_{GS} (it should be taken into account that the external force is opposite to the internal force for the equilibrium configuration).

How could such an optimal external force be reproduced by a simple force pair applied in two atoms? In order to answer this question, a set of external force pairs can be systematically considered by a set of vectors, and projected onto the optimal external force vector, realizing which force pair corresponds to the highest projection.

Molecular Stress–Strain Curve. In order to determine quantitatively what is the range of external forces which can be applied to a certain molecular system (avoiding bond breaking or high interatomic repulsion), single molecule mechanical tests were simulated as follows: considering \mathbf{q}^{eq} as starting structure, the geometry was optimized while constrained at increasingly compressed or elongated interatomic distances (by steps of 0.2 Å), where the pair of atoms selected is the same at which external forces are applied during the dynamics study described above. Nevertheless, contrary to the developed dynamics method, the mechanical properties were calculated by using the true PES, instead of a quadratic expansion around the equilibrium geometries at different external forces. The overall force is then calculated for each optimized structure, having now all elements to obtain a “single molecule stress–strain curve”: the stress σ is defined as force divided by the projection area perpendicular to the applied force vector, based on the van der Waals radius of the molecule;³² the strain corresponds to the deformation of the molecule along the direction of the external force, relative to the initial interatomic length, $\epsilon = l/l_0$ (Figure 2).

In materials science, the relationship between stress and strain is a typical form to characterize macroscopic properties, being unique for each material. In this study, we aimed to characterize microscopic properties of single molecules by a

similar approach, in order to evaluate (as well as in real materials) the Young's modulus E and therefore set the elastic limit, that is, up to which extent the proposed deformation is nonpermanent and hence recoverable, being a necessary information to design molecules with defined optomechanical properties. Moreover, depending on the actual stress–strain curve, plastic region and tensile strength can be estimated (see Figure 2).

Optomechanical Work and Power. The possibility to generate optomechanical work was considered by theorizing a periodic cycle for a photoisomerizable switch involving four consecutive steps, two mechanical and two photoinduced steps: (1) elongation of the molecule initially at state A equilibrium structure due to an external force; (2) electronic excitation of the stretched molecule followed by photoisomerization to state B; (3) recovery of state B equilibrium structure, by removing the elongation force applied in step 1; (4) electronic excitation of state B equilibrium structure to allow photoisomerization back to state A equilibrium structure, therefore closing the cycle. The optomechanical work is straightforward calculated as the area generated by drawing these four steps (linearly approximated) in a graph of force as function of deformation length (Figure 3).

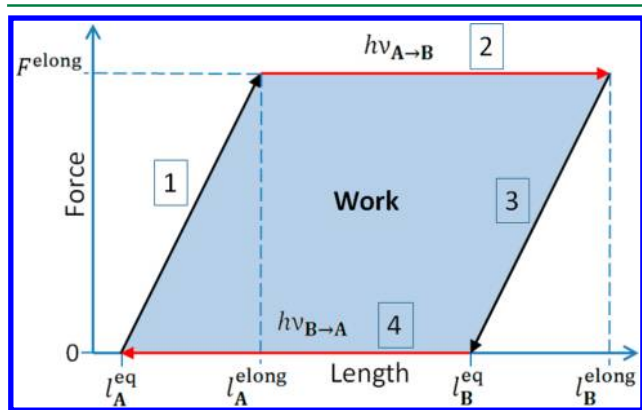


Figure 3. Optomechanical cycle to generate work. Two mechanical steps (1 and 3) and two photoinduced steps (2 and 4) are required, implying application/release of an external elongation force and photoswitching between A and B states, respectively.

The mechanical steps (1 and 3) can be accomplished only if the force applied is within the elastic regime previously calculated by stress–strain curves, otherwise full interconversion between state A and B cannot be ensured, and the periodicity of the optomechanical cycle is not fulfilled.

About the photoinduced steps, while step 4 does not involve any external force, step 2 implies irradiation of the previously stretched molecule, and it is therefore crucial to perform force spectroscopy in order to maximize the absorption and the overall efficiency of the optomechanical cycle.

Once the work is calculated, the optomechanical power can be estimated considering a determined constant frequency, that is, time per cycle accomplished. Especially, the work calculated for a single molecule can be readily amplified if, for example, such a molecule is introduced in the main chain of a polymer (as was already proposed to achieve photoresponsive materials),⁷ hence being of potential interest for design of optomechanical devices.

RESULTS AND DISCUSSION

Azobenzene Topology. The methods described were applied to azobenzene, which is stable in two isomeric forms: *cis* and *trans* (Figure 4). The *trans* isomer is basically planar, being ca. 0.6 eV more stable than the *cis* isomer, due to twisting of the benzene rings around the C–N bond to avoid steric hindrance.³³

The photophysics and photochemistry of this system have been extensively studied: with both (nonpolar) *n*-hexane and (polar) ethanol as solvents, the absorption spectrum shows a $^1(n,\pi^*)$ electronic transition at ca. 430 nm (440 nm) for the *trans* (*cis*) isomer, and a $^1(\pi,\pi^*)$ transition at ca. 320 nm (260 nm) for the *trans* (*cis*) isomer,^{34–38} corresponding to visible and near-UV regions of the spectrum. Concerning the absorption relative intensity, the $^1(\pi,\pi^*)$ transition of *cis*-azobenzene is weaker, but the $^1(n,\pi^*)$ transition is stronger than *trans*-azobenzene³⁸ (see Figure 7). About the photochemistry, isomerization was found to be an ultrafast process for both *cis*-to-*trans* (170 fs) and *trans*-to-*cis* (320 fs) conformational changes.^{17,39} In spite of a large number of experimental and theoretical studies which clarified azobenzene photoisomerization mechanisms and dynamics upon vertical excitation to $^1(n,\pi^*)$ and $^1(\pi,\pi^*)$ states,^{16–20,39–46} few attempts were made to determine accurately the ground state topology.

In a recent work by Klug and Burcl,⁴⁷ the rotational barriers in azobenzene are calculated by Density Functional Theory (DFT) methods, connecting transition states and minima by constrained optimization, starting from a geometry slightly displaced from the transition state geometry along the vibrational eigenvector corresponding to the imaginary frequency. Here, this approach was improved by calculating the reaction path (i.e., by integrating the intrinsic reaction coordinate), hence leading to a minimum energy path description of all rotational barriers. The azobenzene ground state PES is schematically shown by energy levels in Figure 4. It was calculated at the CAM-B3LYP level of theory (i.e., the long-range corrected version of the Becke's three-parameter hybrid exchange functional⁴⁸ with the Lee–Yang–Parr correlation functional,⁴⁹ using the Coulomb-attenuating method⁵⁰), as implemented in Gaussian 09 suite of programs.⁵¹ The 6-311+G(d,p) basis was adopted. Indeed, the CAM-B3LYP functional was shown to correctly describe $^1(n,\pi^*)$ and $^1(\pi,\pi^*)$ states⁵⁰ (see Table 1S in the Supporting Information).

In accordance with previous studies, a transition state structure (TS_{tc}) was found to be responsible for *cis*-to-*trans* thermal isomerization, being characterized by an almost linear N=N–C₁ angle and the phenyl ring containing C₁ perpendicular to the rest of the molecule. By calculating the reaction paths from TS_{tc} we found two previously unreported inflection points (SP_t and SP_c). These structures are characterized, with respect to TS_{tc} by a sort of translation of the perpendicular phenyl ring upward (SP_t) or downward (SP_c) of the N=N bond, starting to define which will be the final isomer. The numerical energy gradient vector was calculated for SP_t and SP_c with different step sizes for differentiation (0.01 Å, 0.02 Å, 0.03 Å), in order to map the sign change of the PES curvature in the proximity of the inflection point: we were able to define only one reaction path for each of the two SP structures, pointing lower in energy and connecting to a transition state that establishes the rotational barrier between the two iso-conformers (TS_t for *trans* and TS_c for *cis*). Actually, a second transition state was found at slightly lower energy (ca.

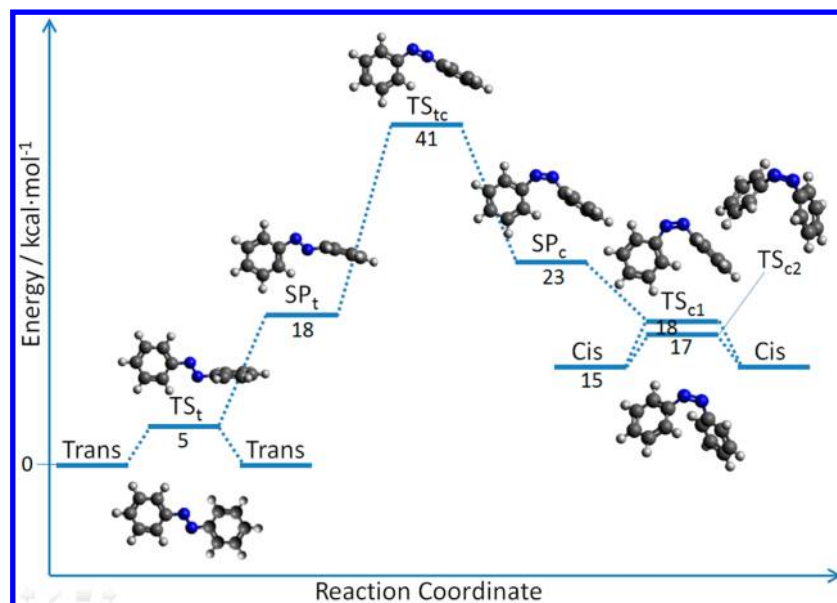


Figure 4. Schematic view of azobenzene ground state potential energy surface.

1 kcal·mol^{−1}) for the *cis* isomer (TS_{c2}), implying a simultaneous rotation of both phenyl rings from the stable (equilibrium) *cis* conformation, in order to reach a symmetric transition state with respect to the N=N bond. As a result, only 5 kcal·mol^{−1} (2 or 3 kcal·mol^{−1}) is required to overcome rotational barriers for the *trans* (*cis*) form, while a considerable energy of 41 kcal·mol^{−1} (26 kcal·mol^{−1}) is needed to undergo a *trans*-to-*cis* (*cis*-to-*trans*) isomerization on the ground state.

An exhaustive study of the ground state topology was considered fundamental in order to evaluate which is the maximum external force which can be applied before a bond is broken, van der Waals contact distance is reached, or, eventually, a mechanically driven isomerization is enforced.

As mentioned in the Methods section, in this study the external force was applied to the two hydrogen atoms of the benzene rings in *para* position with respect to the N=N moiety. In Figure 5 the effect of elongation and compression on the energy of the ground state is schematically represented: on the one hand elongation of the *cis* isomer or compression of the *trans* isomer will determine the minimum force required for mechanical isomerization; on the other hand, elongation of the

trans isomer or compression of the *cis* isomer will result in a constant increase of energy, leading to the maximum force which can be applied before bond breaking or high interatomic repulsion is detected.

Azobenzene Mechanical Properties. The stress–strain curves for elongation and compression tests are shown in Figure 6. The projection area perpendicular to the applied force vector (see Figure 2) is 24.31 Å² for *trans* and 36.74 Å² for *cis* isomers. It results that the minimum force is 5.41 nN for *cis*-to-*trans* and 2.69 nN for *trans*-to-*cis* mechanical isomerization, corresponding to the highest stress recorded for *cis* elongation and *trans* compression curves, respectively. The former result qualitatively agrees with the value found by Shao et al. using the electron-radiation-ion dynamics method, that points toward elongation forces higher than 1.25 nN to produce a pure *cis*-to-*trans* mechanical isomerization (B3LYP/6-31G level of theory).⁸ The maximum force that can be applied before reaching the van der Waals contact distance within the *cis* isomer is 19.50 nN (highest *cis* compression stress), and 6.84 nN before bond breaking of the *trans* isomer (highest *trans* elongation stress).

Among the information that is possible to get from stress–strain curves, we are particularly interested in the Young's modulus, since an optomechanical cycle can be accomplished only if both *cis* and *trans* isomer deformations are within the elastic limit. Interestingly, *E* was found to be much higher for the *trans* isomer (196.9 GPa for elongation, 310.2 GPa for compression) than for the *cis* isomer (8.7 GPa for elongation, 4.4 GPa for compression). We also notice that, even though the overall shape of all the calculated stress–strain curves are typical of thermoplastic materials, the two isomers show distinct features: the *cis* isomer behaves as a semicrystalline thermoplastic, while the *trans* isomer behaves as a glassy (i.e., amorphous) thermoplastic. Indeed, amorphous thermoplastics are usually stiff and brittle, therefore reaching the ultimate tensile strength point at relatively low deformations, following a plateau “rubbery” region at larger deformations (Figure 6, left), while semicrystalline thermoplastics are commonly characterized by larger deformations than amorphous thermoplastics, reaching the ultimate strength point without showing any

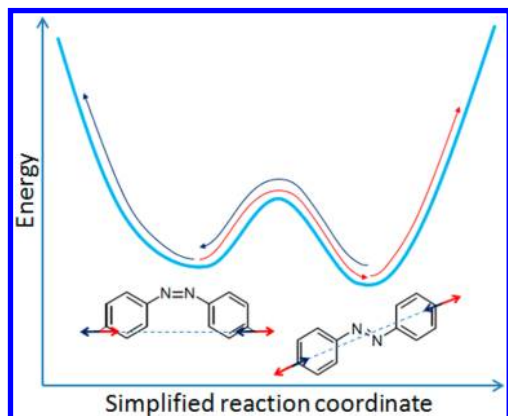


Figure 5. Scheme of compression (blue arrows) and elongation (red arrows) forces applied to azobenzene, with consequent response on a simplified ground state potential energy surface.

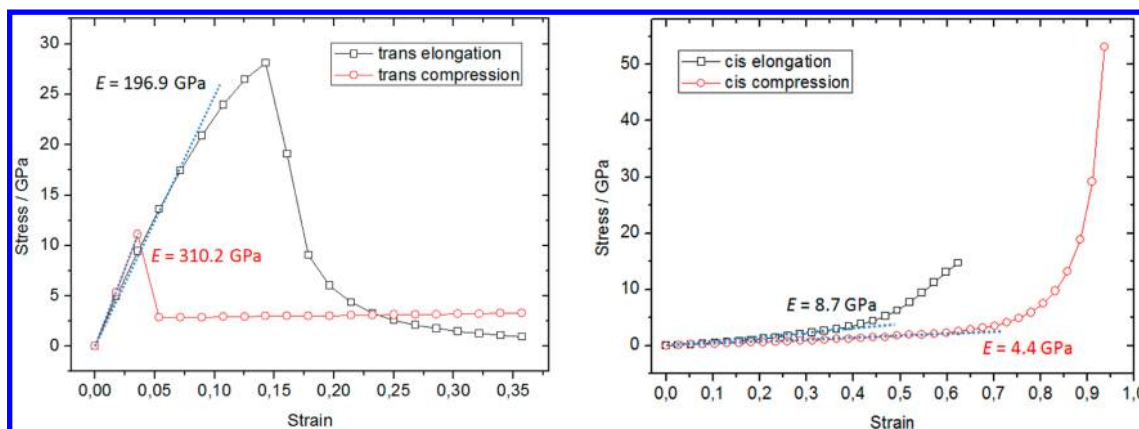


Figure 6. Stress–strain curves for *trans* (left) and *cis* (right) azobenzene isomers. Elongation tests (black) and compression tests (red) with the respective Young's modulus (E) calculated for each elastic region (dashed line) are shown.

“rubbery” region (Figure 6, right).⁵² This could be of interest for the design of photoactive materials, especially photoactive polymers, since physical and engineering properties of thermoplastics (molding performance, behavior of the polymer during processing) mainly depend on their molecular structure.

Azobenzene Force Spectroscopy. The absorption spectra resulting from 1 ns ground state simulations (for a total of 10^7 integration steps) at a temperature of 300 K, obtained when not applying external forces or including a set of different elongation forces, are shown in Figure 7 and Figure 8,

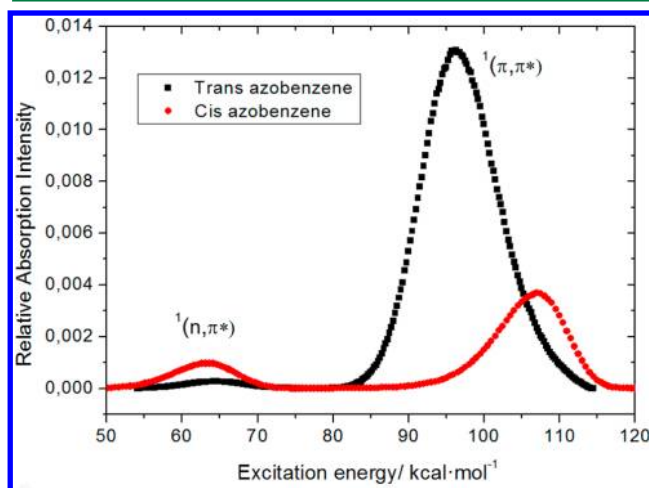


Figure 7. Simulated spectra when not applying external forces (0 nN), for both *cis* (red line) and *trans* (black line) azobenzene. The region of the spectrum assigned to $^1(n,\pi^*)$ or $^1(\pi,\pi^*)$ electronic transitions is shown.

respectively. As expected, the relative absorption is higher for $S_0 \rightarrow S_2$ vertical excitation, corresponding to an optically bright $^1(\pi,\pi^*)$ transition – than for $S_0 \rightarrow S_1$, corresponding to an optically dark $^1(n,\pi^*)$ transition. Moreover, the differences between *cis* and *trans* relative absorption intensities found by experiment (0 nN) are well represented by the simulation.³⁸

In all cases, the applied elongation forces produce a shift of the whole spectrum, with significant differences between the two isomers: the amplitude of the excitation energy shift is considerably larger for *cis*-azobenzene (27–30 kcal·mol^{−1}) than for the *trans* isomer (5–8 kcal·mol^{−1}), allowing a more efficient modulation in the former case. Nevertheless, the *cis*-azobenzene

series of spectra also shows a larger broadening of the peak, especially at forces larger than 2 nN. Moreover, we do observe in all cases a higher relative absorption intensity when applying forces between 1 and 2 nN. This can be explained by the fact that, when compared to 0 nN values, the oscillator strength is higher and, at the same time, the external force is still not large enough to produce a broadening of the peak.

Considering that the applied methodology implies molecular dynamics simulations on an analytical PES built by quadratic expansion (see eqs 1 and 2), a quantitative analysis of the calculated trajectories—within the limits of the method—can be performed by examining ground and excited state Hessian matrices (H_{GS} , H_{ES}) and the energy gradient vector (g_{ES}). Also, a description of negative (imaginary) frequencies is given. The energy difference along g_{ES} provides the first-order correction to E_{exc} , while second-order corrections (orthogonal to g_{ES}) are given by a projected Hessian difference matrix ($H_{ES} - H_{GS}$).⁵³ This allows us to fully understand which internal coordinates are responsible for the excitation energy shift observed.

Looking at $S_0 \rightarrow S_1$ force spectroscopy results (Figure 8 – a, c), a bathochromic shift for both isomers is observed. A single negative frequency is found in S_1 , indicating torsion around the N=N bond (*trans*, -38 cm^{−1}; *cis*, -257 cm^{−1}). When analyzing the projected Hessian difference matrix ($H_{S_1} - H_{S_0}$), the eigenvalues with highest absolute value indicate that C=N=N and N=N=C angles are the most involved internal coordinates. In spite of a similar behavior, the higher frequency found for the *cis* isomer demonstrates that the S_1 PES curvature is larger than for the *trans* isomer, therefore explaining the higher amplitude of the excitation energy shift.

When examining $S_0 \rightarrow S_2$ force spectroscopy results (Figure 8b, d), the most evident difference between the two isomers is about the type of E_{exc} shift: the application of an elongation force provokes a bathochromic shift within *cis*-azobenzene, while a hypsochromic shift was found for *trans*-azobenzene. This can be explained considering S_2 frequencies: two negative frequencies are found for the *trans* isomer, being assigned to torsions around the N=N bond (-244 cm^{−1}) and around both N=C bonds, in opposite directions (-89 cm^{−1}). The same types of frequency modes were found for the *cis* isomer (N=N torsion at -165 cm^{−1} and coupled N=C torsions at -91 cm^{−1}). Nevertheless, additional negative frequencies were recorded for *cis*-azobenzene: -581 cm^{−1}, assigned to N=N stretching, and -1148 cm^{−1}, referring to a complex molecular vibration that couples C=N=N and N=N=C scissoring

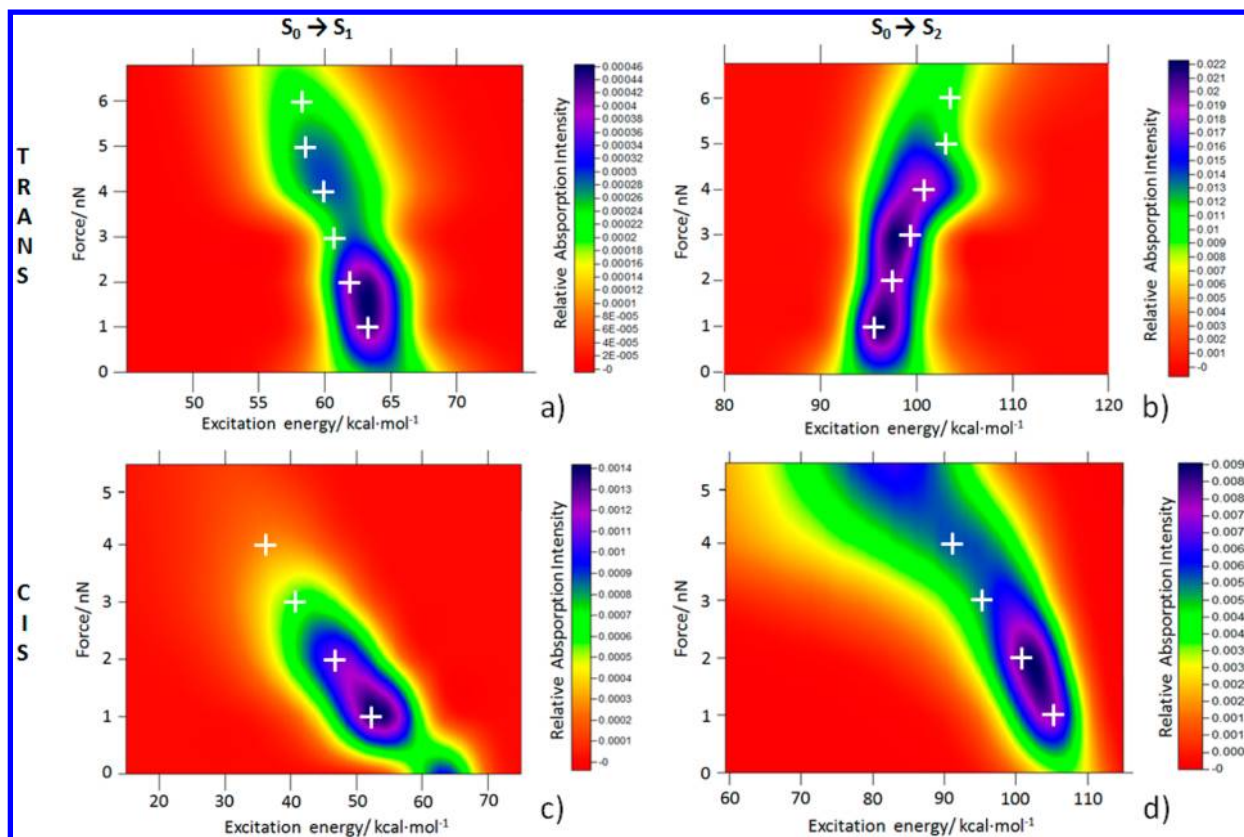


Figure 8. *Trans*- (top) and *cis*- (bottom) azobenzene absorption spectra when applying different elongation forces. The results are shown for $S_0 \rightarrow S_1$ ($^1(n,\pi^*)$) (on the left: a, c) and $S_0 \rightarrow S_2$ ($^1(\pi,\pi^*)$) (on the right: b, d) electronic transitions, by image plots where the relative absorption intensity is color mapped. White crosses indicate the optimized structures under stress.

with stretching of the phenyl moieties along the N—C bond direction. Hence, *trans* and *cis* S_2 PESs are rather different, and this can be further demonstrated by projecting the Hessian difference matrix ($\mathbf{H}_{S_2} - \mathbf{H}_{S_0}$): the eigenvalues related to the *cis* isomer indicate a direct participation of the angles defined by carbon atoms within the phenyl rings. Moreover, as for $S_0 \rightarrow S_1$, the higher frequency values found for the *cis* isomer indicate a larger curvature of the S_2 PES than for the *trans* isomer, again determining a higher amplitude of the excitation energy shift.

Force constrained optimizations are in agreement with the data obtained by dynamics: bathochromic and hypsochromic shifts are qualitatively reproduced, with dynamics underestimating the observed shift in absorption energy.

In order to estimate the error associated with the analytic ground state dynamics, a single point calculation (at the CAM-B3LYP/6-311+G(d,p) level) was performed on 100 geometries randomly selected for each trajectory, and its ground state energy was compared to the predicted energy by correlation graphs: the linear regression R^2 parameters are *ca.* 0.9 or higher for *trans*-azobenzene, while lower R^2 values (0.7–0.8) are recorded for *cis*-azobenzene when applying external forces higher than 1 nN. Nevertheless, in all cases a remarkable correlation was found for the excitation energy ($R^2 \sim 1$; see Supporting Information for details). This could be due to the fact that both ground and excited state energies are affected by almost the same error, finally leading to a correct excitation energy shift.

We should also notice that, since we are considering the intrinsic vibrational fluctuations of the system but neglecting the quantum vibronic states, we may expect nuclear quantum

effects to displace the calculated absorption maxima. Nevertheless, pure quantum dynamics is unaffordable for a large molecule as azobenzene (with 66 internal degrees of freedom). Moreover, we do observe that the main contribution to the broadening of the absorption band is due to stretching modes of the carbon skeleton. Since the vibrational frequency for such kind of modes is of the order of $h\nu \sim kT$, it is not expected to find large differences between the proposed classical dynamics and quantum dynamics. Indeed, our results are in agreement with the experimental absorption spectra recorded without external force.^{37,38}

Compression forces were also considered, finding out that modulation of the absorption energy is limited or, in some cases, not possible at all. More in detail, *trans*-azobenzene shows no modulation for the $S_0 \rightarrow S_1$ transition and a narrow modulation ($3.5 \text{ kcal}\cdot\text{mol}^{-1}$ maximum absorption shift) for the $S_0 \rightarrow S_2$ transition, moreover limited to compression forces not higher than 0.75 nN. The *cis* isomer has a similar behavior, with maximum absorption shifts of $6 \text{ kcal}\cdot\text{mol}^{-1}$ ($S_0 \rightarrow S_1$) and $4 \text{ kcal}\cdot\text{mol}^{-1}$ ($S_0 \rightarrow S_2$), corresponding to a compression force of 0.5 nN. At higher forces no further modulation is recorded (see Supporting Information for details). These findings are in good accordance with experimental results, that report the capability to compress azobenzene (by atomic force microscopy) ensuring *trans*-to-*cis* photoswitching only up to 0.5 nN.⁷

Therefore, elongation would be preferred to compression forces, in order to obtain a higher modulation of the spectroscopical properties and, coupled to a higher deformation, a larger optomechanical work (see Figure 3). As a successful example, a DNA-based molecular motor containing

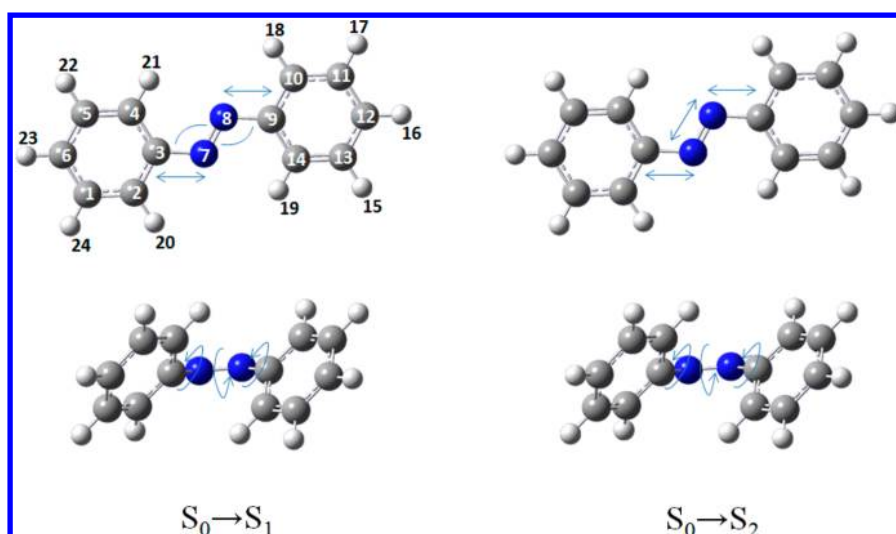


Figure 9. Internal coordinates (blue arrows) most involved in efficient modulation of the $S_0 \rightarrow S_1$ (left) and $S_0 \rightarrow S_2$ (right) excitation energies, for both *trans*- (top) and *cis*- (bottom) azobenzene.

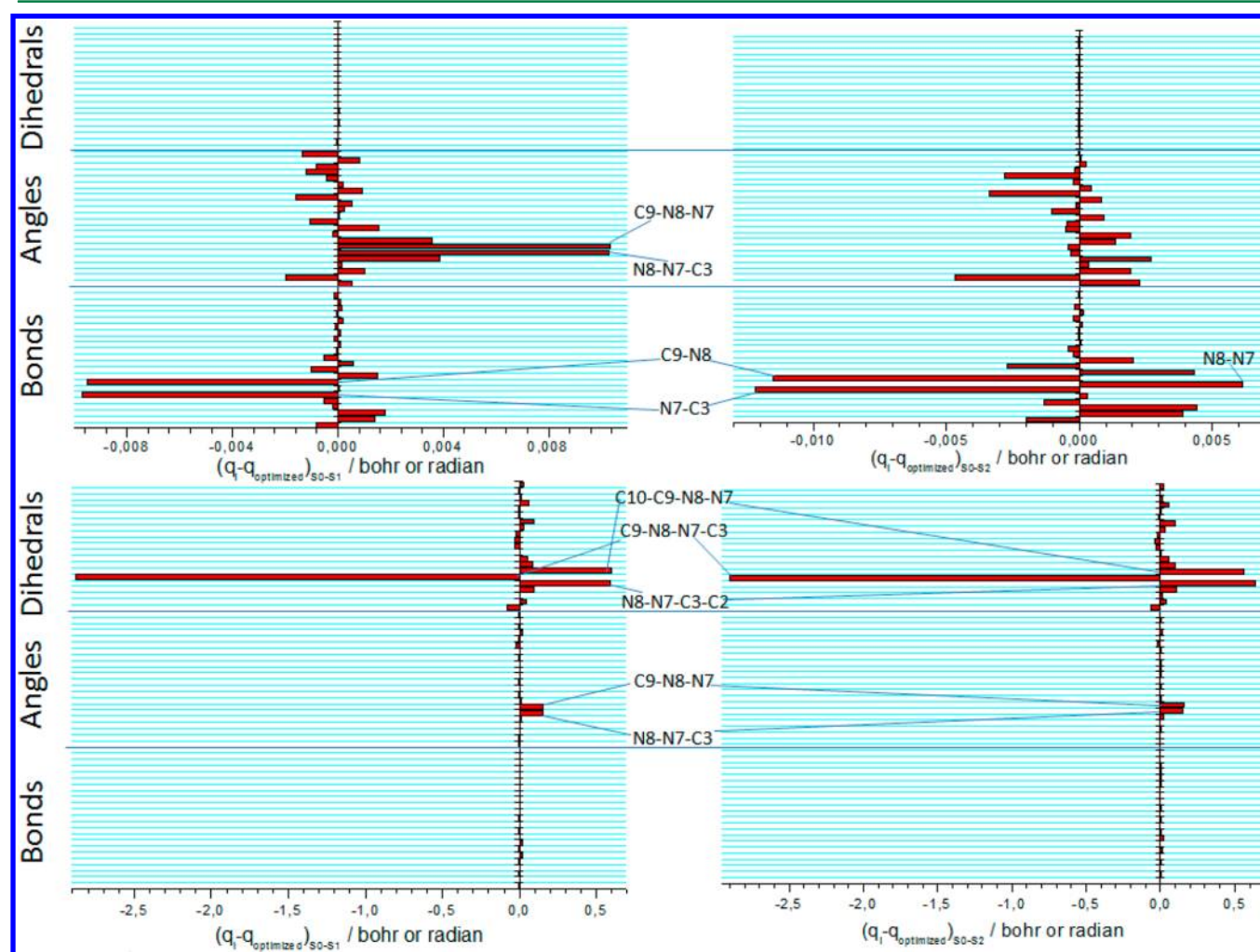


Figure 10. Contributions from each internal coordinate as a function of its variation from the equilibrium geometry (when applying 0.5 nN force), for both $S_0 \rightarrow S_1$ (left) and $S_0 \rightarrow S_2$ (right) vertical excitations. The most relevant coordinates are highlighted, corresponding mainly to angles and bonds for *trans*-azobenzene (top) and to dihedrals for *cis*-azobenzene (bottom). Refer to Figure 9 for atom numbering.

azobenzene as photoswitching unit was already proposed. Nevertheless, in this case the applied elongation forces are strongly limited (elastic limit at *ca.* 0.06 nN) by the fact that the

DNA moiety can undergo unfolding.⁵⁴ We alternatively discuss the eventual inclusion of azobenzene in the main chain of a

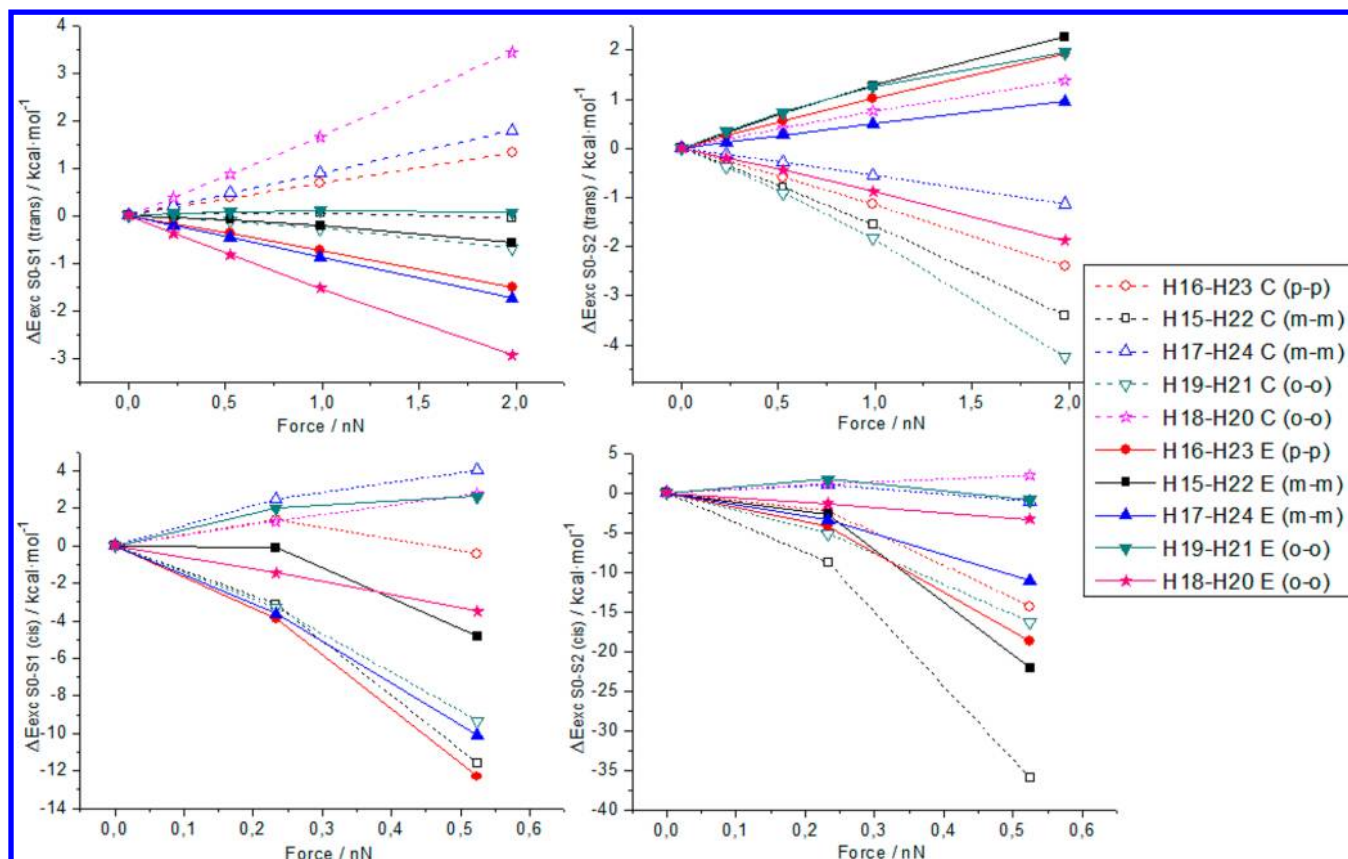


Figure 11. Excitation energy (CAM-B3LYP/6-311+G(d,p) level of theory) modulation as a function of external forces. Compression (C, dotted line) and elongation (E, thick line) is considered for *para-para* (p-p), *meta-meta* (m-m) and *ortho-ortho* (o-o) pair of forces applied to hydrogens (refer to Figure 9 for atom numbering). The results are shown for *trans* (top) and *cis* (bottom) isomers, including $S_0 \rightarrow S_1$ (left) and $S_0 \rightarrow S_2$ (right) electronic transitions.

polymer, where unfolding processes should not play a major role, generating a more convenient optomechanical cycle.

Structural Analysis. In the previous section, the results obtained by applying a pair of forces in *para* position with respect to the N=N moiety were discussed, showing how absorption properties can be modulated by the extent of the force applied. In this section a full structural analysis is performed, in order to determine (1) which molecular distortions are mainly responsible for absorption modulation and (2) which positions within the phenyl ring are the most suitable to efficiently produce such distortions, when a pair of external forces is applied (i.e., considering alternatives to the pair of force vectors in *para-para* configuration). Especially, the main coordinates involved in optimal modulation of the excited state energy gap ($\Delta E_{\text{exc } S_0-S_1}$; $\Delta E_{\text{exc } S_0-S_2}$) are shown in Figure 9, and the role of each internal coordinate is depicted in Figure 10.

We can therefore conclude that the C=N=N-C moiety is responsible for modulation of the excitation energy, being bond stretching and angle bending more relevant for the *trans* isomer, while torsions around dihedral angles are the leading contributions for the *cis* isomer. The variation of the excitation energy per force unit ($\Delta E_{\text{exc}}/F^{\text{ext}}$) is within the range 2–2.5 kcal·mol^{−1}·nN^{−1} in the case of *trans*-azobenzene (up to 4 nN); while for *cis*-azobenzene the highest value (8 kcal·mol^{−1}·nN^{−1}) corresponds to ca. 0.5 nN, and decreases when applying higher forces (see Supporting Information for details).

Different pairs of force vectors were applied in all phenyl positions symmetric with respect to the center of inversion of

the *trans* isomer, resulting in five possibilities: one pair in *para-para*, two pairs in *meta-meta* and two pairs in *ortho-ortho*. The results are shown in Figure 11.

Therefore, even though the application of external forces in *para* positions is a suitable choice (especially for bathochromic shifting the $S_0 \rightarrow S_1$ energy of the *cis* isomer), a more efficient modulation of the absorption energy is usually envisaged by forces applied in *meta-meta* or *ortho-ortho*. Moreover, it is in general possible to select the pair of forces depending on the desired (red or blue) shift, highlighting the red shifting capability of the pair applied at H₁₅–H₂₂ (*meta-meta*) in compression mode to the *cis* isomer ($\Delta E_{\text{exc } S_0-S_2} \sim 36$ kcal mol^{−1}).

Toward a Linear Polymer Photoswitching Device.

Two different operation modes were considered, applying forces at *para* positions (as for the dynamical study). Operation mode I: (1) elongation of the *trans* isomer, (2) *trans-to-cis* photoisomerization, (3) compression of the *cis* isomer, (4) *cis-to-trans* photoisomerization. Operation mode II: (1) elongation of the *cis* isomer, (2) *cis-to-trans* photoisomerization, (3) compression of the *trans* isomer, (4) *trans-to-cis* photoisomerization. Being the elastic limit of *trans*- and *cis*-azobenzene different in force applied and deformation gained, the two proposed operation modes give rise to a different maximum amount of work: operation mode I corresponds to 2.51×10^{-19} J, while operation mode II generates 3.69×10^{-19} J. These values refer to the single molecule. Nevertheless, if we consider n azobenzene units within a linear polymer chain (n : degree of polymerization), an elongation force can be applied

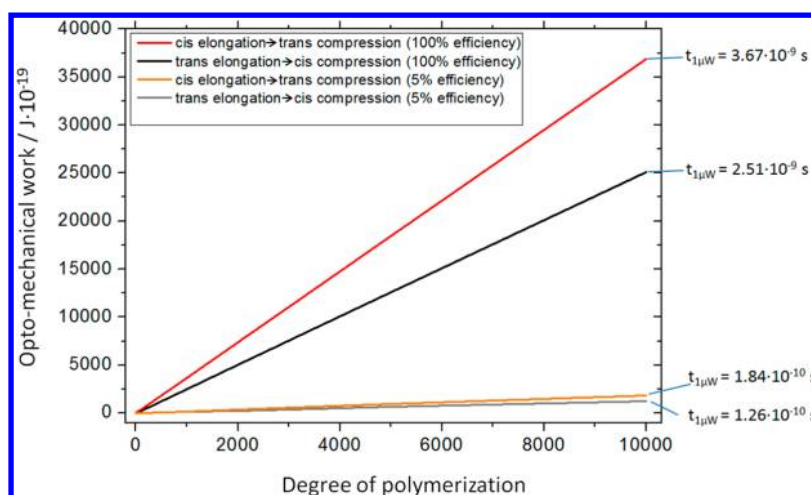


Figure 12. Estimation of the optomechanical work as a function of the degree of polymerization, assuming a linear polymer containing azobenzene units in its main chain. Operation mode I (*trans* elongation \rightarrow *cis* compression) and II (*cis* elongation \rightarrow *trans* compression) are shown, for a total efficiency of 100% and 5%, that takes into account the photoisomerization quantum yield during the cycle. For a 10 000 degree polymerization, the time required to perform a cycle in order to generate 1 μ W power is calculated.

to both ends of the chain, producing an overall deformation n times larger with respect to the single molecule (assuming that all azobenzene units are in the same isomeric form). Experimentally, different methods were successfully applied in order to synthesize and characterize polymers bearing azobenzene moieties in their main chain.^{13,21–24} Therefore, once clarified the optomechanical behavior of the single monomer, the work can be considered as a linear function of the degree of polymerization (Figure 12). This straightforward calculation corresponds to a device able to fully convert the optical excitation energy into mechanical work. Nevertheless, to complete a single optomechanical cycle a 5% quantum yield was experimentally estimated for azobenzene photoisomerization,^{7,55} reducing the overall efficiency of the eventual device (see Figure 12). Especially, the work estimated by Holland et al. for an oligomer containing 10 azobenzene units, resulting from a first compression step (0.4 nN), is $ca. 5 \times 10^{-20}$ J.⁵⁵ In our work, the corresponding oligomer operating in modes I and II (i.e., undergoing elongation as first step) would correspond to $ca. 12 \times 10^{-20}$ J and 18×10^{-20} J, respectively, being a notable improvement.

Moreover, assuming a certain degree of polymerization and setting a target value for the power that could be produced by such a motor, the time required to perform an optomechanical cycle can be estimated. For example to obtain 1 μ W power (scale of interest in nanotechnology⁵⁶), a time between 1 and 2×10^{-10} s would be required by a linear polymer chain containing 10 000 azobenzene units, with a realistic efficiency of 5% (Figure 12).

Considering that azobenzene photoisomerization was proven to be an ultrafast process for both *cis*-to-*trans* (0.17 ps) and *trans*-to-*cis* (0.32 ps) conformational changes,^{17,39} a full optomechanical cycle of $ca. 0.5$ ps (1 ps = 10^{-12} s) can be estimated, leading to a low degree of polymerization to accomplish the requirements of a 1 μ W motor: 40 in operation mode I and 27 in operation mode II. Increasing to 10000 the degree of polymerization, the corresponding power scales up to $ca. 251 \mu$ W (mode I) and 369μ W (mode II).

As future perspectives, we can define four parameters by which work (and therefore power) can be improved: (i) degree of polymerization, (ii) maximum force applicable, (iii)

maximum deformation (elongation and compression) length, (iv) quantum yield of the photoisomerization. While the first is a macromolecular parameter involving polymer chemistry, the other three parameters are characteristics of the single chromophore.

SUMMARY AND CONCLUSIONS

We presented new methodologies to simulate force spectroscopy experiments on single molecules, on the basis of optimization and classical dynamics on analytical potential energy surfaces. Large simulations (nanosecond time scale) were performed at a low computational cost, in order to reproduce electronic absorption spectra while applying a constant external force to both ends of the chromophore under study.

The proposed method was applied to azobenzene, one of the most studied photoswitches. Its mechanical properties were investigated by reproducing the corresponding stress–strain curves. This allowed to estimate the elastic limit and therefore the maximum forces which could be applied during the force spectroscopy simulations.

The resulting absorption spectra have shown the possibility to modulate the vertical excitation energy as a function of the elongation force and of the position within the molecule where it is applied, for both *trans* and *cis* isomers. This could be of interest for laser applications and optomechanical devices. Especially, we calculated the work generated by performing a single molecule optomechanical cycle, applying two different operation modes. After a comparison with available results in literature, an optomechanical motor based on a linear polymer bearing azobenzene units in its main chain was discussed, finally estimating the work and power eventually produced as a function of the degree of polymerization. Interestingly, we observe the possibility to produce power in the microwatt scale even at low degrees of polymerization.

ASSOCIATED CONTENT

Supporting Information

Absorption spectra while applying compression forces. Details of the developed methodologies. Analysis of the errors related to the ground and excited state energies. Numerical evaluation

of the oscillator strength. Cartesian coordinates of the most relevant structures along the ground state minimum energy path. Cartesian coordinates of the force constrained optimized structures. This material is available free of charge via the Internet at <http://pubs.acs.org>.

AUTHOR INFORMATION

Corresponding Authors

*Tel.: +34 91 885 2512. Fax: +34 918854763. E-mail: luisma.frutos@uah.es.

*E-mail: marco.marazzi@uah.es.

Present Address

[†]Department of Theoretical Chemical Biology, Institute for Physical Chemistry, Karlsruhe Institute of Technology, Kaiserstr. 12, 76131 Karlsruhe, Germany

Notes

The authors declare no competing financial interest.

ACKNOWLEDGMENTS

This research was supported by the Spanish MICINN grants CTQ2009-07120 and CTQ2012-36966. F.Z. is grateful to the Spanish MEC (Ministerio de Educación y Ciencia), and M.A.F.-G., D.R., and M.M. are grateful to the UAH (Universidad de Alcalá) for a doctoral fellowship.

DEDICATION

This work is dedicated to Prof. Obis Castaño on the occasion of his 70th birthday.

REFERENCES

- (1) Hosono, N.; Kajitani, T.; Fukushima, T.; Ito, K.; Sasaki, S.; Takata, M.; Aida, T. *Science* **2010**, *330*, 808.
- (2) Bleger, D.; Yu, Z.; Hecht, S. *Chem. Commun.* **2011**, *47*, 12260.
- (3) *Molecular Switches*; 2nd ed.; Feringa, B. L.; Browne, W. R., Eds.; Wiley-VCH: Weinheim, 2011.
- (4) *Molecular Devices and Machines*; 2nd ed.; Balzani, V.; Credi, A.; Venturi, M., Eds.; Wiley-VCH: Weinheim, 2008.
- (5) García-Iriepa, C.; Marazzi, M.; Frutos, L. M.; Sampedro, D. *RSC Adv.* **2013**, *3*, 6241.
- (6) Turansky, R.; Konopka, M.; Doltsinis, N. L.; Stich, I.; Marx, D. *ChemPhysChem* **2010**, *11*, 345.
- (7) Hugel, T.; Holland, N. B.; Cattani, A.; Moroder, L.; Seitz, M.; Gaub, H. E. *Science* **2002**, *296*, 1103.
- (8) Shao, J.; Lei, Y.; Wen, Z.; Dou, Y.; Wang, Z. *J. Chem. Phys.* **2008**, *129*, 164111/1.
- (9) Turansky, R.; Konopka, M.; Doltsinis, N. L.; Stich, I.; Marx, D. *Phys. Chem. Chem. Phys.* **2010**, *12*, 13922.
- (10) Doltsinis, N. L.; Marx, D. *J. Theor. Comput. Chem.* **2002**, *1*, 319.
- (11) Blanco-Lomas, M.; Samanta, S.; Campos, P. J.; Woolley, G. A.; Sampedro, D. *J. Am. Chem. Soc.* **2012**, *134*, 6960.
- (12) Schierling, B.; Noel, A.-J.; Wende, W.; Hien, L. T.; Volkov, E.; Kubareva, E.; Oretskaya, T.; Kokkinidis, M.; Roempp, A.; Spengler, B.; Pingoud, A. *Proc. Natl. Acad. Sci. U. S. A.* **2010**, *107*, 1361.
- (13) Sapich, B.; Vix, A. B. E.; Rabe, J. P.; Stumpe, J. *Macromolecules* **2005**, *38*, 10480.
- (14) Ercole, F.; Davis, T. P.; Evans, R. A. *Polym. Chem.* **2010**, *1*, 37.
- (15) Mahimwalla, Z.; Yager, K. G.; Mamiya, J.-i.; Shishido, A.; Priimagi, A.; Barrett, C. J. *Polym. Bull. (Heidelberg, Ger.)* **2012**, *69*, 967.
- (16) Satzger, H.; Root, C.; Braun, M. *J. Phys. Chem. A* **2004**, *108*, 6265.
- (17) Naegle, T.; Hoche, R.; Zinth, W.; Wachtveitl, J. *Chem. Phys. Lett.* **1997**, *272*, 489.
- (18) Fujino, T.; Tahara, T. *J. Phys. Chem. A* **2000**, *104*, 4203.
- (19) Fujino, T.; Arzhantsev, S. Y.; Tahara, T. *J. Phys. Chem. A* **2001**, *105*, 8123.
- (20) Chang, C.-W.; Lu, Y.-C.; Wang, T.-T.; Diao, E. W.-G. *J. Am. Chem. Soc.* **2004**, *126*, 10109.
- (21) Huang, H.-Y.; Lee, Y.-T.; Yeh, L.-C.; Jian, J.-W.; Huang, T.-C.; Liang, H.-T.; Yeh, J.-M.; Chou, Y.-C. *Polym. Chem.* **2013**, *4*, 343.
- (22) Jaycox, G. D. *J. Polym. Sci., Part A: Polym. Chem.* **2005**, *44*, 207.
- (23) Keum, C.-D.; Ikawa, T.; Tsuchimori, M.; Watanabe, O. *Macromolecules* **2003**, *36*, 4916.
- (24) Howe, L. A.; Jaycox, G. D. *J. Polym. Sci., Part A: Polym. Chem.* **1998**, *36*, 2827.
- (25) Davis, D. A.; Hamilton, A.; Yang, J.; Cremer, L. D.; Van, G. D.; Potisek, S. L.; Ong, M. T.; Braun, P. V.; Martinez, T. J.; White, S. R.; Moore, J. S.; Sottos, N. R. *Nature* **2009**, *459*, 68.
- (26) Kryger, M. J.; Ong, M. T.; Odom, S. A.; Sottos, N. R.; White, S. R.; Martinez, T. J.; Moore, J. S. *J. Am. Chem. Soc.* **2010**, *132*, 4558.
- (27) Lenhardt, J. M.; Ong, M. T.; Choe, R.; Evenhuis, C. R.; Martinez, T. J.; Craig, S. L. *Science* **2010**, *329*, 1057.
- (28) Wolinski, K.; Baker, J. *Mol. Phys.* **2009**, *107*, 2403.
- (29) Wolinski, K.; Baker, J. *Mol. Phys.* **2010**, *108*, 1845.
- (30) Tuckerman, M. E.; Liu, Y.; Ciccotti, G.; Martyna, G. J. *J. Chem. Phys.* **2001**, *115*, 1678.
- (31) Martyna, G. J.; Tuckerman, M. E.; Tobias, D. J.; Klein, M. L. *Mol. Phys.* **1996**, *87*, 1117.
- (32) *Marvin 5.12.0*; ChemAxon: Budapest, Hungary, 2013; www.chemaxon.com.
- (33) Brown, E. V.; Granneman, G. R. *J. Am. Chem. Soc.* **1975**, *97*, 621.
- (34) Lednev, I. K.; Ye, T. Q.; Matousek, P.; Towrie, M.; Foggi, P.; Neuwahl, F. V. R.; Umaphathy, S.; Hester, R. E.; Moore, J. N. *Chem. Phys. Lett.* **1998**, *290*, 68.
- (35) Lednev, I. K.; Ye, T.-Q.; Hester, R. E.; Moore, J. N. *J. Phys. Chem.* **1996**, *100*, 13338.
- (36) Hamm, P.; Ohline, S. M.; Zinth, W. *J. Chem. Phys.* **1997**, *106*, 519.
- (37) Hamon, F.; Djedaini-Pillard, F.; Barbot, F.; Len, C. *Tetrahedron* **2009**, *65*, 10105.
- (38) Bandara, H. M. D.; Burdette, S. C. *Chem. Soc. Rev.* **2012**, *41*, 1809.
- (39) Ishikawa, T.; Noro, T.; Shoda, T. *J. Chem. Phys.* **2001**, *115*, 7503.
- (40) Pederzoli, M.; Pittner, J.; Barbatti, M.; Lischka, H. *J. Phys. Chem. A* **2011**, *115*, 11136.
- (41) Toniolo, A.; Ciminelli, C.; Persico, M.; Martinez, T. J. *J. Chem. Phys.* **2005**, *123*, 234308/1.
- (42) Cembran, A.; Bernardi, F.; Garavelli, M.; Gagliardi, L.; Orlandi, G. *J. Am. Chem. Soc.* **2004**, *126*, 3234.
- (43) Monti, S.; Orlandi, G.; Palmieri, P. *Chem. Phys.* **1982**, *71*, 87.
- (44) Ciminelli, C.; Granucci, G.; Persico, M. *Chem.—Eur. J.* **2004**, *10*, 2327.
- (45) Gagliardi, L.; Orlandi, G.; Bernardi, F.; Cembran, A.; Garavelli, M. *Theor. Chem. Acc.* **2004**, *111*, 363.
- (46) Conti, I.; Garavelli, M.; Orlandi, G. *J. Am. Chem. Soc.* **2008**, *130*, 5216.
- (47) Klug, R. L.; Burcl, R. *J. Phys. Chem. A* **2010**, *114*, 6401.
- (48) Becke, A. D. *J. Chem. Phys.* **1993**, *98*, 1372.
- (49) Lee, C.; Yang, W.; Parr, R. G. *Phys. Rev. B: Condens. Matter* **1988**, *37*, 785.
- (50) Yanai, T.; Tew, D. P.; Handy, N. C. *Chem. Phys. Lett.* **2004**, *393*, 51.
- (51) Frisch, M. J.; Trucks, G. W.; Schlegel, H. B.; Scuseria, G. E.; Robb, M. A.; Cheeseman, J. R.; Scalmani, G.; Barone, V.; Mennucci, B.; Petersson, G. A.; Nakatsuji, H.; Caricato, M.; Li, X.; Hratchian, H. P.; Izmaylov, A. F.; Bloino, J.; Zheng, G.; Sonnenberg, J. L.; Hada, M.; Ehara, M.; Toyota, K.; Fukuda, R.; Hasegawa, J.; Ishida, M.; Nakajima, T.; Honda, Y.; Kitao, O.; Nakai, H.; Vreven, T.; Montgomery, J. A., Jr.; Peralta, J. E.; Ogliaro, F.; Bearpark, M.; Heyd, J. J.; Brothers, E.; Kudin, K. N.; Staroverov, V. N.; Kobayashi, R.; Normand, J.; Raghavachari, K.; Rendell, A.; Burant, J. C.; Iyengar, S. S.; Tomasi, J.; Cossi, M.; Rega, N.; Millam, J. M.; Klene, M.; Knox, J. E.; Cross, J. B.; Bakken, V.; Adamo, C.; Jaramillo, J.; Gomperts, R.; Stratmann, R. E.; Yazyev, O.; Austin, A. J.; Cammi, R.; Pomelli, C.; Ochterski, J. W.; Martin, R. L.;

Morokuma, K.; Zakrzewski, V. G.; Voth, G. A.; Salvador, P.; Dannenberg, J. J.; Dapprich, S.; Daniels, A. D.; Farkas, O.; Foresman, J. B.; Ortiz, J. V.; Cioslowski, J.; Fox, D. J. *Gaussian 09*, Revision D.01; Gaussian, Inc.: Wallingford, CT, 2009.

(52) *Thermoplastics and Thermoplastic Composites*; 1st ed.; Biron, M., Ed.; Elsevier Ltd.: Oxford, 2007.

(53) Fernandez-Gonzalez, M. A.; Marazzi, M.; Lopez-Delgado, A.; Zapata, F.; Garcia-Iriepe, C.; Rivero, D.; Castano, O.; Temprado, M.; Frutos, L. M. *J. Chem. Theory Comput.* **2012**, *8*, 3293.

(54) McCullagh, M.; Franco, I.; Ratner, M. A.; Schatz, G. C. *J. Am. Chem. Soc.* **2011**, *133*, 3452.

(55) Holland, N. B.; Hugel, T.; Neuert, G.; Cattani-Scholz, A.; Renner, C.; Oesterhelt, D.; Moroder, L.; Seitz, M.; Gaub, H. E. *Macromolecules* **2003**, *36*, 2015.

(56) Wang, Z. L.; Wu, W. *Angew. Chem., Int. Ed.* **2012**, *51*, 11700.